



HAL
open science

Temporal Structured Classification of Sentinel 1 and 2 Time Series for Crop Type Mapping

Sébastien Giordano, Simon Bailly, Loic Landrieu, Nesrine Chehata

► **To cite this version:**

Sébastien Giordano, Simon Bailly, Loic Landrieu, Nesrine Chehata. Temporal Structured Classification of Sentinel 1 and 2 Time Series for Crop Type Mapping. 2018. hal-01844619

HAL Id: hal-01844619

<https://hal.science/hal-01844619v1>

Preprint submitted on 19 Jul 2018

HAL is a multi-disciplinary open access archive for the deposit and dissemination of scientific research documents, whether they are published or not. The documents may come from teaching and research institutions in France or abroad, or from public or private research centers.

L'archive ouverte pluridisciplinaire **HAL**, est destinée au dépôt et à la diffusion de documents scientifiques de niveau recherche, publiés ou non, émanant des établissements d'enseignement et de recherche français ou étrangers, des laboratoires publics ou privés.

Temporal Structured Classification of Sentinel 1 and 2 Time Series for Crop Type Mapping

Sébastien Giordano^a, Simon Bailly^a, Loic Landrieu^a, Nesrine Chehata^{b,a}

^aUniv. Paris-Est, LASTIG MATIS, IGN, ENSG, F-94160 Saint-Mande, France

^bEA 4592, G&E Lab, Bordeaux INP/ Bordeaux Montaigne University, France

Abstract

As part of the EU Common Agricultural Policy (CAP) reform of 2020, each EU member country is expected to suggest new farmland management protocols. Currently, farmers must manually declare each year their crop types into the Land-Parcel Identification Systems (LPIS), a geographic information system identifying the land use of agricultural parcels within each EU member country. Such a protocol remains tedious and error-prone. Automatic Earth observation image analysis can help achieving such a task. Leveraging the recent availability of precise and frequent Sentinel acquisitions, this work aims to automate the LPIS update.

We propose modeling the crop type of parcels from a sequence of (radar and optical) satellite acquisitions, as well as LPIS entries of previous years, with a linear-chain Conditional Random Field. The novelty lies on the fusion of multi-modal images at the feature level and the integration of temporal knowledge extracted from existing land-cover databases. We tested our model on two large-scale French study areas ($\geq 1250 \text{ km}^2$), which are geographically distant and show different agronomic rules: the *Seine et Marne* (North of France) and the *Alpes de Haute-Provence* (South East). We use a granular nomenclature comprised of 25 categories.

Our model demonstrates promising results for the task of automating the LPIS update: 89.0% overall accuracy is reached in *Seine et Marne* (10 categories of the 25 present on the area) and 72.9% in *Alpes de Haute-Provence* (14 categories). We show that the temporal modeling increases the accuracy by +2.6% and +4.6%, respectively.

Keywords: classification, temporal regularization, conditional random fields, agriculture, monitoring, Sentinel images

32 1. Introduction

33 1.1. Motivation

34 The Sentinel 1&2 satellites provide open and free acquisitions exhibiting
35 unprecedented characteristics which are perfectly tailored to agriculture
36 monitoring. Most critically, the high temporal frequency (5-6 days) is very
37 beneficial for identifying crop types. The Sentinel program will be maintained
38 at until at least 2030, which allows us to chronicle both short and long-term
39 evolutions. Besides, the multispectral Sentinel-2 images display relevant
40 spectral bands to agricultural monitoring, that are complementarity to C-
41 Band Sentinel-1 radar images. Finally, the high spatial resolution of both
42 optical and radar images (10-20 m) authorizes parcel-level approaches. For
43 all these reasons, the European Commission strongly recommended the use of
44 the Sentinel programme for reshaping the procedures to monitor the Common
45 Agricultural Policy (CAP) European Commission [1]. This therefore becomes
46 a significant line of research in the forthcoming decade.

47 In Europe, several use-cases of agricultural monitoring using Sentinel
48 images have been proposed [1], such as crop monitoring (crop area estimates,
49 crop map products, crop phenology indicators), controlling CAP payments
50 with remote sensing (permanent grasslands, greening measures, . . .), updating,
51 and controlling the quality of the Land Parcel Identification System (LPIS)
52 or precision farming at the farm-level.

53 In this paper, we focus on *automating crop type mapping*. In Europe,
54 the agricultural land cover information is manually updated yearly by the
55 farmers themselves. They input the type and surface area of their parcels.
56 This manual declaration is complicated for farmers, error-prone and leads to
57 expensive control procedures by external agencies. In this context, a pre-filled
58 agricultural declaration based on supervised classification techniques would
59 allow the farmers to only have to validate the declaration, cutting down on
60 control and input errors. The automation of crop type declarations requires
61 a robust classification model, based on Sentinel images observations but also
62 on ancillary data such as LPIS archives to improve the classification results.

63 Indeed, the crop type identification may be improved using *a priori*
64 knowledge on management practices and especially on crop rotations per
65 parcel. The choice of the crop type and agricultural practices on a parcel are
66 strongly dependent on past events over previous years. The LPIS archives
67 provide such information. Modeling these temporal structures in combination

68 with the Sentinel image time series can lead to significant gains in classification
69 accuracy. In this paper, we focus on benefiting from *crop rotation knowledge*.

70 1.2. Related work

71 1.2.1. Multi-temporal satellite images for crop mapping

72 In the literature, many studies showed the potential of multi-temporal
73 satellite images for crop type mapping [2]. Inglada et al. [3] assessed state-
74 of-the-art methods for automatic crop mapping with multi-temporal and
75 very high spatial resolution optical images. For this purpose, five different
76 classification approaches using SPOT4 and Landsat-8 images were compared
77 on 12 different study areas worldwide. Best results (Overall accuracy of 80%
78 for 6 annual crop classes) were obtained with the Random Forest classifier [4].
79 Immitzer et al. [5] used mono-temporal Sentinel-2 images for agricultural and
80 forest land cover classification. A multi-temporal approach has been proposed
81 by Kussul et al. [6]. Landsat-8 and Sentinel-1 time series were used on a study
82 area in Ukraine. A pixel-based classification accompanied with a parcel-based
83 regularization (majority voting) was proposed using LPIS ancillary data. An
84 overall accuracy of 89% was reached but the nomenclature was limited to 6
85 annual crops (Winter wheat, Winter rapeseed, Maize, Sugar beet, Sunflower,
86 Soybeans) and large parcels were generally considered (> 250 ha). More
87 recently, experiments were led at the country level (Czech Republic) by the
88 Sen2-Agri consortium [7]. A multi-sensor (Sentinel-1, Sentinel-2) pixel-based
89 supervised classification was performed. The LPIS was used for both learning
90 and validation steps. A crop map was produced every month using Sentinel-1
91 radar images (December to September) and Sentinel-2 optical images (March
92 to September). The overall accuracy was greater than 80% and each land
93 cover type had a F-score greater than 60%. The quality of the classification
94 was further increased as more data was acquired. However, the nomenclature
95 was here again very limited (7 classes) and does not fully integrate temporal
96 knowledge from existing data.

97 Two major aspects of the state-of-art of crop type classification remain to
98 be improved in order to obtain a reliable pre-filled declaration system: the
99 precision on small parcels and the granularity of the nomenclature.

100 1.2.2. Crop rotation consideration

101 Crop rotations are known to be useful management practices, improving
102 agricultural yields [8] and soil quality [9]. References in literature on their role
103 in agriculture are numerous [10]. To take into account crop rotations in crop

104 type prediction, two questions have to be answered: (i) how to model the crop
105 rotations? (ii) how to integrate crop rotations in a land cover classification
106 process?

107 1.2.3. Modeling crop rotations

108 Two different approaches can be used to model rotations. The first one
109 consists in using *a priori* agronomist expert knowledge. The second one
110 would be to automatically learn crop rotations from the statistical analysis of
111 past practices, as found in the LPIS archives. The crop rotation knowledge
112 can then be modeled with a common representation in agronomy: transition
113 matrices representing transition probabilities between crop types from year
114 to year.

115 The ROTAT model [11] is based on expert knowledge. The tool automati-
116 cally generates all possible crop rotations over an area and performs a selection
117 taking expert knowledge into account. Castellazzi et al. [12] introduce a math-
118 ematical framework based on transition matrices to model crop rotations at
119 the landscape scale. Dury et al. [13] review various crop rotation models
120 and emphasize that these models are too static. To improve the models,
121 the authors propose integrating different time scale dynamics. Indeed, crop
122 rotation models have several limitations. The information is never available
123 at the parcel scale. The models are strongly dependent on the study area;
124 they cannot adapt to environmental or agricultural management changes.
125 Some studies have been proposed to overcome these limitations. Aurbacher
126 and Dabbert [14] underline the importance of having rotation information at
127 the parcel-level and consequently propose to use Markov chains. Concerning
128 adaptation capacities to different study areas, Detlefsen and Jensen [15] use
129 network modeling techniques to find on a given parcel the optimal rotations
130 knowing a selection of crops. Finally, the influence of environmental changes
131 such as global warming on agricultural practices has been studied by Olesen
132 et al. [16], then modeled by Aurbacher et al. [17]. Nevertheless, few studies
133 take this parameter into account in crop rotation models.

134 Learning rotations using past data on crop types is a way of overcoming
135 the limitations of *a priori* expert knowledge approaches. Both approaches can
136 also be successfully combined. For instance, the CarrotAge tool [18] allows to
137 perform a spatio-temporal analysis by training a Hidden Markov Models with
138 a land cover database. Results are thereafter interpreted by an agronomist in
139 order to be integrated in soil or water management studies. Another example
140 is the CropRota method [19] that combines agronomic criteria and land cover

141 information to generate crop models at the farm or region levels. The ROTOR
142 model [20] relies on control sampled farms, field surveys and expert knowledge.
143 These three models can take into account changes in agricultural practices or
144 study areas. However, expert knowledge is still required, and such models
145 can not be used at the parcel level.

146 The parcel-level crop information provides a finer crop type nomenclature
147 but needs heavy field surveys and more complex models than those described
148 above. Xiao et al. [21] used such parcel-based information to describe the
149 spatial distribution of crop sequences at a large regional scale, but with a
150 limited 3-class nomenclature. For many years, several European countries
151 as well as the United States maintain and annually update a geographical
152 information system on agricultural parcels, i.e. the Land Parcel Identification
153 System (LPIS) [22]. Parcel-based crop rotation information at a national scale
154 can be derived by exploiting past annual versions of the LPIS. The information
155 on environmental or agricultural changes is then implicitly contained in these
156 data. Several studies proposed to use the LPIS to study and model crop
157 rotations. Leteinturier et al. [23] used several years of LPIS to compute crop
158 rotation indicators. More recently, Osman et al. [24] produced and assessed a
159 land cover classification based on the former version of the French LPIS.

160 *1.2.4. Integrating crop rotations into classification pipelines*

161 Only few studies have focused on the integration of crop rotation infor-
162 mation into classification pipelines. Osman et al. [24] studied early crop
163 mapping using only the LPIS. A prediction model based on Markov logic was
164 proposed, but not in combination with remote sensing observations. Results
165 showed that this model has better classification precision than models based
166 on remote sensing observations at the beginning of the crop growing season.
167 This is mainly due to the fact that few satellite images are available at the
168 beginning of growing season and that crops are hard to distinguish at this
169 development stage: observation-based classification is unreliable compared
170 to temporal prediction. This statement remains to be confirmed with the
171 use of higher temporal resolution Sentinel images. Other studies proposed
172 to introduce a temporal structure, using the Hidden Markov Chains, in a
173 classification pipeline but they aim at modeling phenology instead of crop
174 rotations [25, 26, 27]. Modeling phenology is useful to detect optimal temporal
175 intervals to acquire remote sensing images for crop mapping [28]. Kenduiywoa
176 et al. [29] modeled phenology information into a Conditional Random Field,
177 but the classification is performed at different dates through the year.

178 *1.3. Specific objectives*

179 The general objective of this article is to assess the feasibility of a pre-filled
180 agricultural declaration based on Sentinel 1+2 images for crop types and
181 surfaces. This paper focuses on crop type predictions. Related work described
182 in Section 1.2, allow us to formulate the following specific objectives:

- 183 • **Thematic contribution.** Sentinel images are part of a recent satellite
184 program (October 2014 and December 2015 for radar and optical images,
185 respectively). Few research studies have yet assessed the crop type
186 prediction accuracies that could be obtained with these time series.
187 This study will especially focus on using an exhaustive national crop
188 nomenclature, the consideration of all agricultural parcels (with no
189 minimal crop area consideration), and the complementarity between
190 Sentinel-1 and Sentinel-2 images.
- 191 • **Methodological contribution.** Crop rotations have rarely been com-
192 bined with satellite observations into a classification pipeline. Our
193 objective is to propose a method that integrates the crop rotation tem-
194 poral structure into the classification process and to assess the capacity
195 of the proposed method to improve crop type prediction accuracies.

196 Sentinel data, LPIS, and the study sites will be described in Section 2 as
197 well as the necessary image and vector preprocessing steps. Two study sites
198 with very different agricultural management practices and parcel sizes are
199 chosen. In Section 3, we propose a parcel-based classification with a Random
200 Forest classifier [4] and a temporal-structured framework to integrate crop
201 rotation information. Results are given and discussed in Section 4. The
202 models learned for the LPIS crop rotations and land cover prediction from
203 the Sentinel images are first assessed independently. A combination of both
204 models is finally evaluated and discussed.

205 **2. Site and material**

206 *2.1. Study sites*

207 In order to assess the feasibility of a pre-filled declaration of crop types, two
208 complementary large-scale sites were chosen in France. The characteristics
209 and location of each site are provided in Figure 1 and Table 1.

210 The first one is located in South Eastern France, in the Alpes de Haute-
211 Provence region, in the Durance river Valley. It is representative of a Mediter-
212 ranean cultivated area. This site will be called *Site04* in reference to the
213 national number of the corresponding region. It covers 1050 km² and is
214 characterized by a highly variable topography, a very fragmented parcellar
215 while giving a high diversity of crop types. The site is an observatory of the
216 French mapping agency (IGN) where crop observations are made annually.

217 The second one is located near Paris, in the Seine et Marne region, at the
218 north of Coulommiers town. It covers 233 km². Contrarily to the *Site04*, this
219 site is characterized by a flat relief, with a large parcellar and a majority of
220 cereal crops. This site is a permanent observatory of a Group of Scientific
221 Interest; GIS Oracle (<http://gisoracle.irstea.fr/>). This site will be
222 noted *Site77* in reference to the national number of the corresponding region.

223 Table 1 illustrates the difference of both sites in terms of covered area and
224 cultivated crop types. Figure 3 gives for both sites the normalized histograms
225 of parcels area. Figures 4 and 5, show *Site04* and *Site77*, respectively, with
226 the corresponding parcels and nomenclatures.

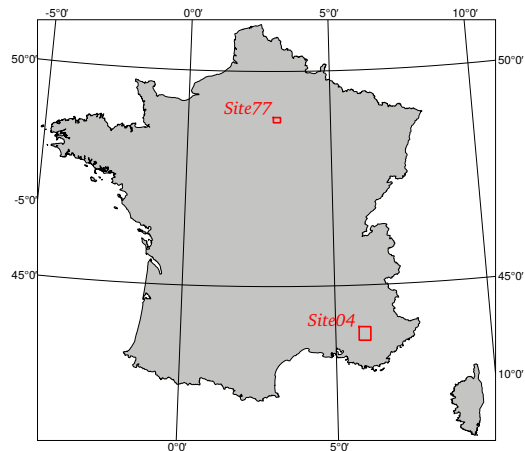


Figure 1: Localisation of *Site04* and *Site77*

227 2.2. Land Parcellar Identification system

228 In France, the Land Parcellar Identification System is called *Registre*
229 *Parcellaire Graphique* (RPG). It is available on the whole territory since 2002.
230 It corresponds to a Geographic Information System (GIS) of cultivated and

231 non cultivated areas (NCA) that may correspond to isolated trees, hedges,
 232 groves, artificial areas . . . For cultivated areas, the RPG gathers the geometric
 233 information (i.e., the parcel delimitation) and the corresponding semantic
 234 information allowing to identify each agricultural parcel such as the owner,
 235 the operator, the area, the crop type etc (*cf.* Figure 2).

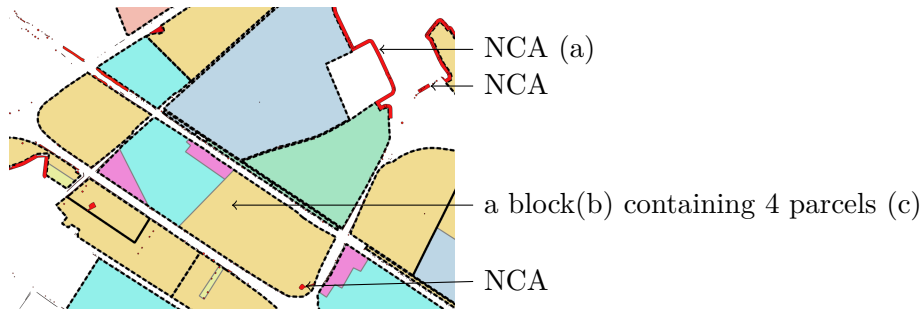


Figure 2: Details of the French LPIS (RPG). (a) Non cultivated areas (NCA); (b) a block of contiguous parcels, belonging to the same operator (dashed lines); (c) a Parcel, defined by its owner, operator, surface, crop type. . .

236 All this information has to be entered in April-May period for each year
 237 by the farmers. Until 2014, the declarations were made at a parcel block scale
 238 for contiguous parcels with the same operator. Since 2015, the declarations
 239 are made at the parcel scale. The crop type is specified among more than
 240 300 sub-classes, which are organized into 28 classes. This study focuses on a
 241 parcel-based approach. Thus, to be in tune with Sentinel-2 images availability,
 242 only the 2016 parcel-based RPG edition is used for training and validation.
 243 The geometrically stable blocks of parcels from 2010 to 2014 (available LPIS
 244 data) were used to learn crop rotations. The latter step was processed on the
 245 corresponding departments of both sites ((77): 5915 km² and (04): 6925 km²),
 246 in order to get more robust crop type transitions.

247 2.3. Nomenclature

248 The 28-class nomenclature used in the RPG declarations is driven agri-
 249 cultural monitoring needs: hence, it exhibits a fine-grained categorization.
 250 However, some classes are indistinguishable from purely remote sensing obser-
 251 vations, such as lands left in fallow for different amount of times. Consequently,
 252 we present in Table 1 a slightly adjusted nomenclature of 25 classes. 14 and
 253 10 of these classes are present on *Site04* and *Site77*, respectively.

Class	# parcels - <i>Site04</i>	# parcels - <i>Site77</i>
Corn	147	350
Barley	517	158
Other cereals	2176	889
Rape seed	154	85
Sun flower	293	✗
Other oilseeds	116	✗
Protein(peas)	87	76
Fiber plants	✗	76
Forage crops	1215	46
Meadows	3652	725
Fruit trees	298	30
Vignards	249	✗
Olive groves	1029	✗
Aromatic crops	1452	✗
Vegetables	520	131
Total nb classes	14	10
Total nb parcels	11905	2566
Site area (km^2)	1050	233
Total nb stable parcels 2015/2016	9230	1902
Total transitions 2010-14	29478	36891

Table 1: Comparison of both study sites in terms of area and crop types.

254 Figure 3 shows the distribution of parcel sizes on both sites. One can see
255 that *Site04* is much more fragmented with very small parcels while *Site 77*
256 shows large parcels reaching 20 ha.

257 Figures 4 and 5 show the 2016 RPG edition i.e., the ground truth data
258 on *Site04* and *Site77* respectively, with the corresponding classes on each
259 site. One can observe that, on *Site04*, dominant crops are: *cereals* (23.8%),
260 *meadows* (30.7%), *aromatic crops* (12.2%), *forage crops* (10.2%) and *olive*
261 *groves* (8.6%). For *Site77*, two dominant crops are present: *cereals* (57.7%),
262 *meadows* (28.3%), followed by *vegetables* (5.1%). The data are much more
263 imbalanced in the latter case, making the *77* classification task more complex.

264 2.4. Multimodal Sentinel-1 & Sentinel-2 images

265 Our framework is fed with multimodal and temporal Sentinel images
266 dedicated to agricultural applications and environmental monitoring. The

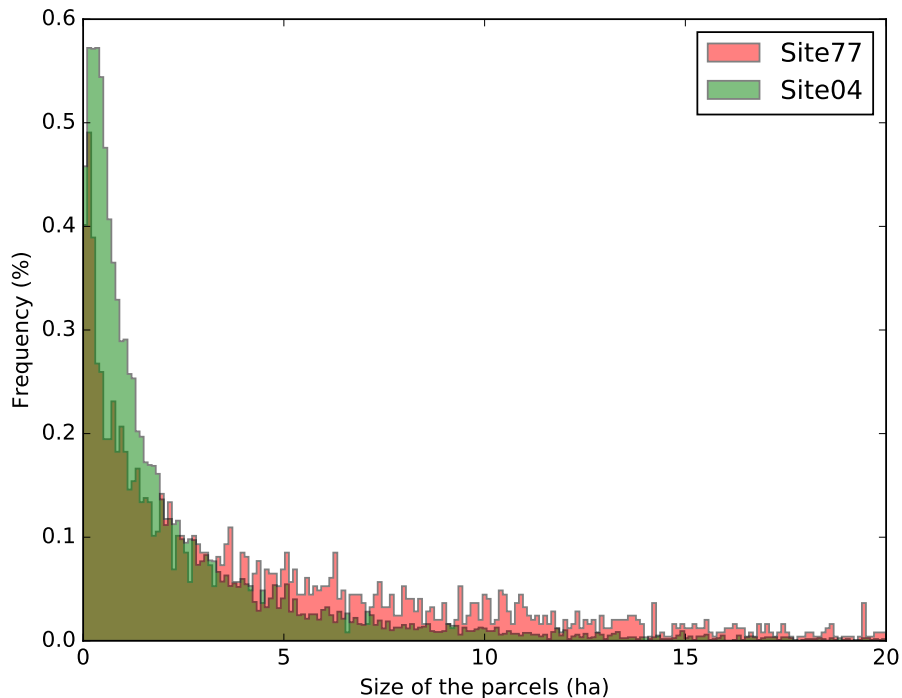


Figure 3: Normalized histogram of parcel area for *Site04* and *Site77*.

267 high spectral resolution of the images and high temporal sampling rate
 268 make these acquisitions particularly well-suited for crop mapping (Table 2).
 269 Sentinel-1 (S1) sensor provides band-C SAR images while Sentinel-2 (S2)
 270 provides multispectral images.

271 Figure 6 shows a Sentinel-2 optical and a Sentinel-1 radar acquisitions on
 272 *Site04*, more precisely on *Oraison* Village.

273 Sentinel-2 (S2) is a multispectral sensor with 13 bands covering the VIS-
 274 SWIR domain, which measures the reflectance of surface objects in different
 275 optical domains. In particular, its near infra-red (NIR) and red-edge bands
 276 allow a fine characterization of crops. Sentinel-1 is a C-band SAR. This allows
 277 to measure scattering coefficients that are related to an emitted waveform
 278 ($\lambda = 5.5$ cm in C-band). The recorded energy depends on the characteristics of
 279 the encountered object (slope, roughness, humidity, etc.) and on the emitted
 280 waveform (wavelength, polarization). Sentinel-1 has different acquisition

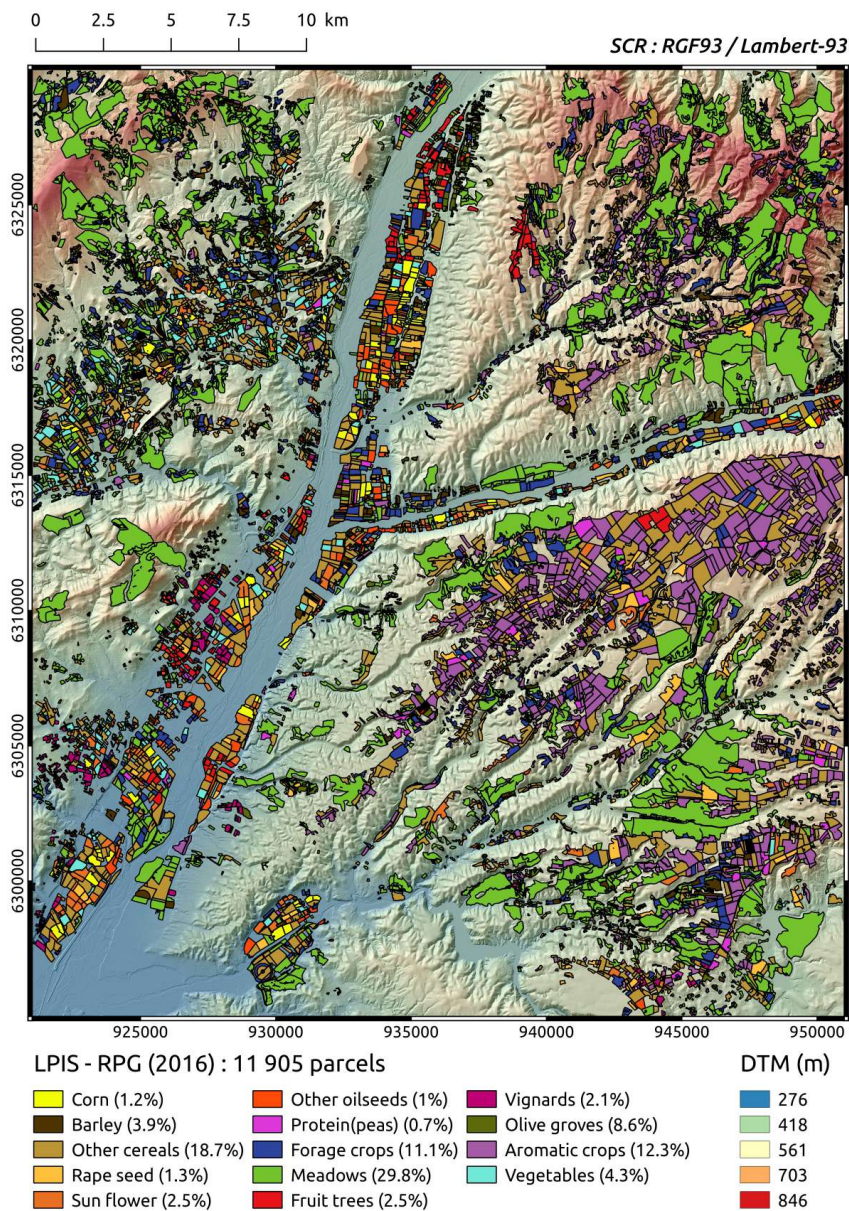


Figure 4: *Site04*: 2016 RPG parcellar superimposed to a very high resolution Digital Terrain Model.

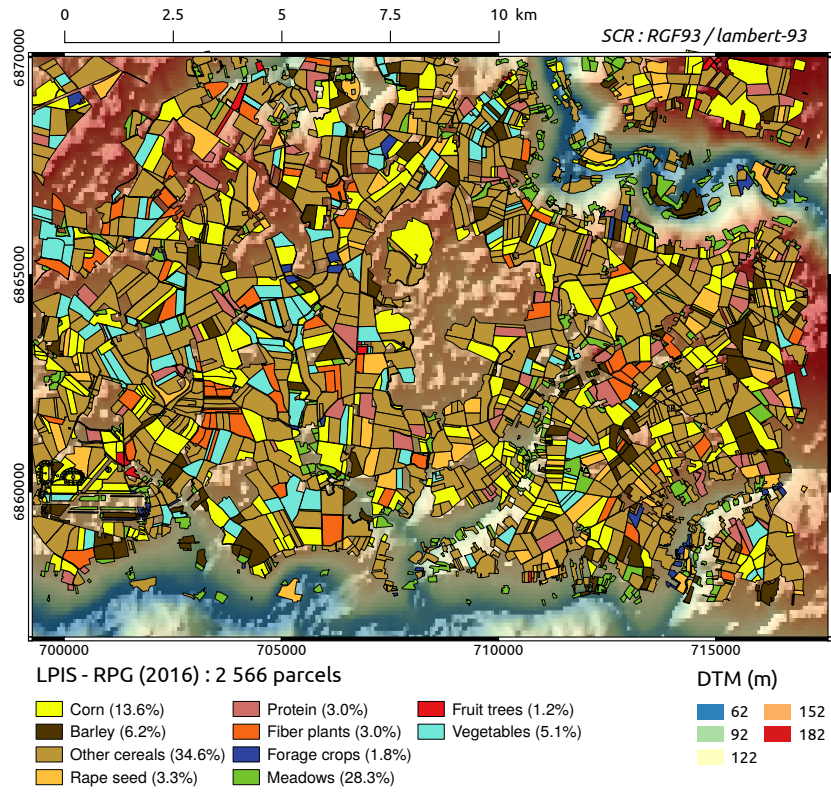


Figure 5: *Site77*: 2016 RPG parcellar superimposed to a SRTM Digital Terrain Model.

	Acquisition date	Sensor	Characteristics
Sentinel-1	3 April 2014 (S1A) 25 April 2016 (S1B)	C-SAR (5,4 GHz)	Cycle: 12 jours # satellites: 2 (S1A et S1B) Revisit period: 6 days Resolution: 5-20 m by default (mode IW) Polarization: dual (VV,VH)
Sentinel-2	23 June 2015 (S2-A) 7 March 2017 (S2-B)	Multispectral image	Cycle: 10 days # satellites: 2 (S2A et S2B) Revisit period: 5 days Resolution: 10 m - 60 m according to band Spectral: 13 bands (2 NIR and 3 Red-edge)

Table 2: Characteristics of Sentinel sensors and used images: Sentinel-1, Sentinel-2.

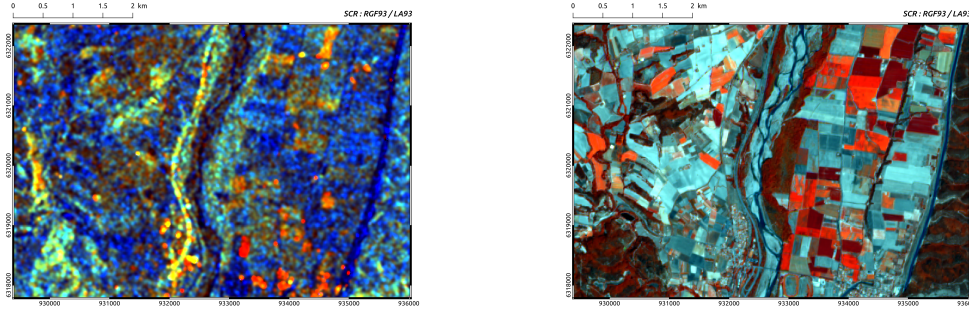


Figure 6: *Site04*, focus on Oraison village: Sentinel-1 (5 Aug. 2015). Composed color image with different polarizations related to retrodiffusion coefficients: σ_{vv} , σ_{vh} , $\frac{\sigma_{vh}}{\sigma_{vv}}$. Site04-Oraison village: Color-infrared Sentinel-2 (3 Aug. 2015). See text for more details.

281 modes that differ according to observed surface, sensor spatial resolution and
 282 polarization. The available mode on the studied sites was the Interferometric
 283 Wide (IW) mode. This mode presents a dual polarization:

- 284 • VV : Incident waveform is polarized vertically and the antenna records it
 285 vertically. This polarization allows us to characterize the soil roughness.
- 286 • VH : Incident waveform is polarized vertically and the antenna records
 287 it horizontally. This polarization provides volumetric information on
 288 vegetation.

289 In addition, we use directly the GRD (*Ground Range Detected*) image
 290 format, which corresponds to the average of approximately five Single Look
 291 Complex ((SLC) acquisitions corrected by the incidence angle and resampled
 292 at 10 m spatial resolution (Section 2.5.2).

293 2.5. Sentinel image pre-processing

294 Figure 7 illustrates the optical and radar pre-processing steps to obtain
 295 parcel-based features that will be fed into our classification workflow.

296 2.5.1. Sentinel images repositories

297 Sentinel images are available on several platforms: the *Copernicus scihub*
 298 (<https://scihub.copernicus.eu/>) at the European level, the scihub mirror
 299 *Peps* (<https://peps.cnes.fr>) and the downstream service *Theia* (<https://www.theia-land.fr/>) at the French national level. Sentinel-2 images (10
 300 bands) were automatically downloaded from the *Theia* platform as they were
 301

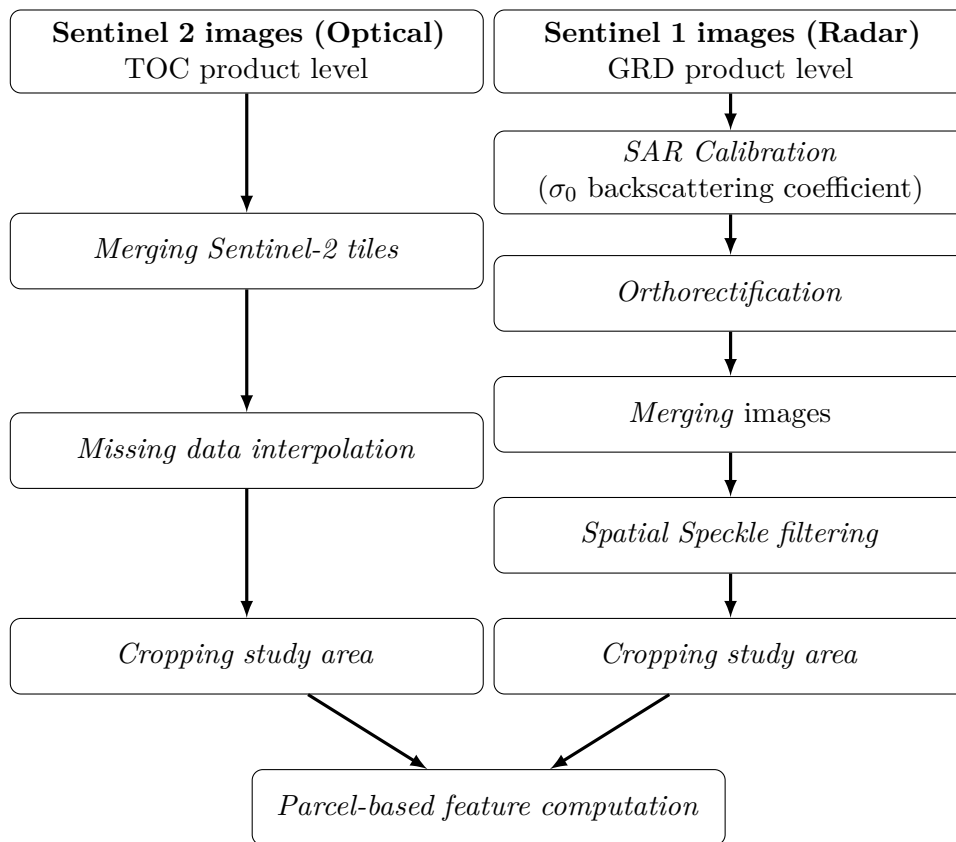


Figure 7: Sentinel-1 and 2 pre-processing steps

302 available in tiled format, calibrated as Top of Canopy (TOC) reflectance and
 303 accompanied with robust cloud mask information. Radar Sentinel-1 images
 304 were downloaded from the *Peps* platform in the Ground Range Detected
 305 format (GRD). The total number of images is illustrated in Table 3 and
 306 confirms the complementarity between Sentinel-1 and Sentinel-2 images, where
 307 the latter may suffer from an important cloud cover while Sentinel-1 radar
 308 images allow to get more information. For instance, on *Site77*, particularly
 309 obstructed by cloudy skies, Sentinel-2 images (12) are 7 times fewer than the
 310 S1 images (85). On the particular Sentinel-2 orbit covering the *Site77* study
 311 area, many acquisition problems occurred in 2016. On the contrary, *Site77*
 312 is located where ascendant Sentinel-1 images overlap making the available
 313 radar images more numerous.

314 *2.5.2. Sentinel 1 pre-process*

315 The dual polarization GRD S1 images were first calibrated to σ_0 radar
 316 backscattering coefficient. Then, the orthorectification was performed using
 317 the SRTM digital terrain model and the georeferencing information supplied
 318 with the GRD files. The speckle is partly removed using a simple 5×5
 319 Lee filter [30]. The information was then averaged at the parcel level. In
 320 addition to VV and VH radar features, an extra radar feature ($\frac{\sigma_{0VH}}{\sigma_{0VV}}$) was
 321 derived. This ratio is known to be more robust to acquisition system errors
 322 or environmental factors such as soil moisture. As a result, Veloso et al.
 323 [31] argue that it is a more temporal stable indicator than the σ_{0VV} et σ_{0VH}
 324 backscattering coefficient.

325 Average and standard deviation of these three features per radar image
 326 are then computed for each date and for each parcel of the study sites. The
 327 number of obtained features are shown in Table 3 .

Site	Nb of dates	Optical features	Radar features	Total
04	Optical: 23	20 per image	6 per image	Optical: 460
	Radar: 28	(σ and μ of 10 bands + NDVI)	(σ and μ of 3 radar features)	Radar: 168 total: 628
77	Optical: 12	20 per image	6 per image	Optical: 240
	Radar: 85	(σ and μ of 10 bands)	(σ and μ of 3 radar features)	Radar: 509 total: 749

Table 3: Characteristics of the parcel-based features for both sites. See text for more details.

328 *2.5.3. Sentinel 2 pre-process*

329 Sentinel-2 images downloaded from *Theia* platform were already orthorec-
 330 tified in a cartographic system and calibrated in TOC reflectance. When the
 331 study area covered more than one tile, the corresponding tiles and cloud masks
 332 were merged. On *Site77*, only 12 Sentinel-2 optical images were obtained
 333 in 2016 as shown in Figure 8 with corresponding cloud cover whereas 23
 334 images are available on *Site04*. The missing data (clouds) were filled using a
 335 multi-temporal spline interpolation [32]. Average and standard deviation of
 336 the 10 spectral bands per optical image were then computed for each date
 337 and for each parcel of the study sites. The number of obtained features are
 338 shown in Table 3.

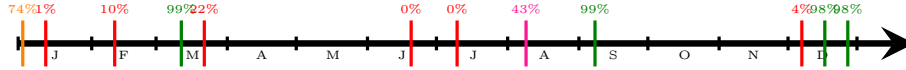


Figure 8: S2 optical images over the year 2016 and corresponding cloud cover on *Site77*.

339 2.6. LPIS pre-process

340 Seven editions of the French LPIS were used. From 2010 to 2014, the crop
 341 type is defined at the block level (Figure 2) (i.e., the majority crop type of
 342 the block) with a nomenclature of 28 classes. For 2015 and 2016 editions, the
 343 crop type is known at the parcel-level with a detailed nomenclature (over 300
 344 classes). In order to use all available editions, all LPIS were aggregated to
 345 the 25 considered classes. Geometrically stable parcels were identified using
 346 a GIS spatial join between 2015 and 2016 versions. The number of stable
 347 parcels for both sites is given in Table 1. The 2016 stable parcels were used
 348 for training and validation of the supervised classification model (Section 3.1).
 349 The 2015 stable parcels were necessary to train the temporal structured
 350 method (Section 3.2). Finally, a similar GIS spatial join was performed at
 351 the block level for 2010-2014 LPIS editions, over the whole corresponding
 352 regions (04 and 77) in order to get more robust crop transitions. Thus, a
 353 5-year series of crop type transitions were obtained on stable blocks over both
 354 04 and 77 regions. The number of transitions for each study site is given in
 355 Table 1. These transitions will be used in the temporal structure estimation
 356 (Section 3.2.1).

357 3. Methodology

358 Our method can be broken down into two components: parcel-wise clas-
 359 sification and temporal modeling. The first part aims to predict the crop
 360 types per parcel using Sentinel time series with no temporal structure. The
 361 second component consists in integrating into a structured model the temporal
 362 structure derived from previous LPIS editions and based on crop rotations.

363 3.1. Parcel-based multi-source classification

364 The first step in our pipeline is crafting discriminative features from
 365 sequential satellite acquisitions. For each parcel, we consider all available
 366 (and interpolated) optical and radar data over one year. To obtain parcel-
 367 based rather than pixel-based features, we consider the average and standard

368 deviation of each spectral band over the pixels composing the parcel. Those
 369 attributes are aggregated into a tensor of dimensions equal to twice the
 370 number of acquisitions over the year for each parcel.

371 We then perform feature selection by iteratively removing the features
 372 with the least *importance* until the cross-validated classification score starts
 373 decreasing over our learning set. For a given parcel i and a given year t
 374 we denote $X_i^{(t)} \in \mathbb{R}^D$ the tensor of aggregated selected features, with D the
 375 selected feature size. As certain classes were over-represented in our data sets,
 376 each class is weighted proportionally to the square root of the inverse of its
 377 number of instances.

378 A Random Forest classifier is selected for the classification task. It provides
 379 parcel-wise prediction under the form of a pseudo-probability.

380 3.2. Temporal-structured classification of parcels

381 We now consider the temporal structure of each parcel independently. We
 382 denote by $X_i \in \mathbb{R}^{T \times D}$ the sequence of features $X_i^{(t)} \in \mathbb{R}^d$ for the parcel i for
 383 the years $t = 1, \dots, T$. Likewise, we denote $Y \in \mathcal{K}^{N \times T}$ the labels of each
 384 parcel for each observed year with \mathcal{K} the set of all possible labels.

385 3.2.1. Temporal structure

386 The aim of this step is to model the yearly crop rotations in order to
 387 improve crop type prediction.

As stated in 1.2.2, crop rotation has a significant impact on land cover. This dependency is modeled with a discriminative linear chain Conditional Random Field (CRF) of order m , as shown in Figure 9. For a parcel i , we model the posterior distribution $P(Y_i | X_i)$ of the labels Y_i given the observed features X_i as:

$$P(Y_i | X_i) = \frac{1}{Z} \exp \left(\sum_{t=1}^T O(Y_i^{(t)}, X_i) + \sum_{t=m+1}^T I(Y_i^{(t-m)}, \dots, Y_i^{(t)}, X) \right), \quad (1)$$

where Z is a normalizing factor, O the observation potential, and I the interaction potential, described below.

Observation potential: The observation potential models the link between the observed features and the label of each parcel. $O(Y_i^{(t)}, X_i)$ is taken as the logarithm of the pseudo-probability given by the random forest classifier, described in Section 3.1.

Interaction potential: This potential models the temporal dependencies

between the parcel's labels. We model this potential as the transition probability from a sequence $Y_i^{(t-m)}, \dots, Y_i^{(t-1)}$ to a label $Y_i^{(t)}$. For the sake of simplicity, we choose an homogeneous parameterization, independent of the observed features, and shared by all parcels and years:

$$I(Y_i^{(t-m)}, \dots, Y_i^{(t)}, X) = \log \left(M(Y_i^{(t-m)}, \dots, Y_i^{(t)}) \right),$$

388 with $M \in \mathbb{R}_+^{k^m}$ a tensor such that $\sum_{\{i_1, \dots, i_{m-1}\} \in \mathcal{K}^{m-1}} M_{i_1, \dots, i_{m-1}, i_m} = 1$ for all
 389 $i_m \in \mathcal{K}$. This tensor can be interpreted as a transition probability from a
 390 sequence in \mathcal{K}^{m-1} to a label in \mathcal{K} [33].

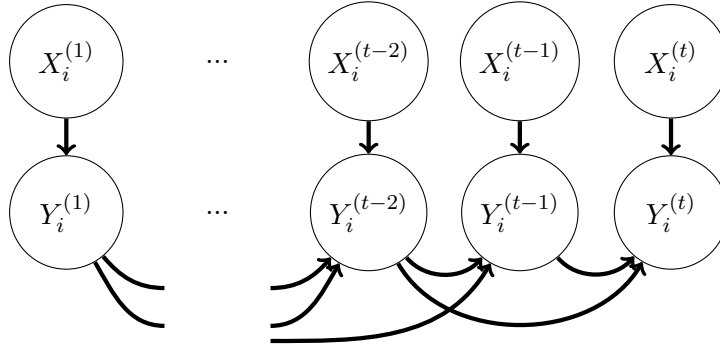


Figure 9: Graph structure of the temporal dependency at order 2.

391 3.3. Learning

The observation potential is obtained by training the random forest classifier. Learning the transition tensor \hat{M} from labeled data can be done in close form. For $i_1, \dots, i_m \in \mathcal{K}^m$, let:

$$\hat{M}_{i_1, \dots, i_m} = \frac{N_{i_1, \dots, i_m}}{N_{i_1, \dots, i_{m-1}}},$$

392 with N_{i_1, \dots, i_m} the number of sequences i_1, \dots, i_m observed in the labeled data
 393 for all parcels and all years, and $N_{i_1, \dots, i_{m-1}}$ the number of sequences i_1, \dots, i_{m-1}
 394 observed for the $T - m$ first years.

395 To account for the large size of this matrix (k^m) and to prevent numeric
 396 issues, we perform a Laplacian smoothing with $\alpha = 1$ as described in Manning
 397 et al. [34, 11.3.2].

398 *3.4. Inference*

The aim of this step is to predict the label $Y_i^{(t)}$ from the labels and observations of the previous years for an unseen parcel. This can be directly computed by injecting the observation and interaction potentials obtained from the trained models into

$$p(Y_i^{(t)} = k | Y_i^{(t-m, \dots, t-1)}, X_i) \propto \exp \left(O(k, X_i^{(t)}) + I(Y_i^{(t-m)}, \dots, Y_i^{(t-1)}, k) \right),$$

399 and normalizing the results to obtain a probability.

400 **4. Results and discussions**

401 In this section, we present the experimental setup and the evaluation
402 metrics. Results are illustrated on both sites and will be discussed with
403 regard to methodological and thematic objectives presented in Section 1.3.

404 *4.1. Experimental setup*

405 The random forest classifier is composed of 100 decision trees. The
406 meta-parameters of the forest, such as the maximum number of attributes
407 considered at each node, are chosen by k -fold cross-validation with $k = 4$.

408 For the temporal structure, spatio-temporal homogeneity hypothesis al-
409 lows us to estimate the transition tensor \hat{M} . For each study site, only the
410 geometrically-stable parcel-blocks over the corresponding departments and a
411 period of 5 years are used. The number of 5-year transitions that contribute
412 to estimate \hat{M} is given in Table 1.

413 The data is randomly split equally into a training and a testing sets. In
414 practice, the availability of numerous LPIS editions allows us to have a high
415 number of training parcels. The model is trained and validated on the training
416 set while the quality of the model is estimated on the testing set. The overall
417 accuracy (OA) is used to assess the general performance of the model, while
418 the F-score for each class allows us to estimate the per-class quality. To sum
419 up this information, the F-scores are averaged, with and without weighting
420 by the class cardinality. The results are given as an average over 10 runs of
421 the random forest classifier.

422 *4.2. Transition matrix assessment*

423 The transitions were computed on geometrically stable parcels between
424 2010-2014. In this study, only first order transitions were computed, i.e.,

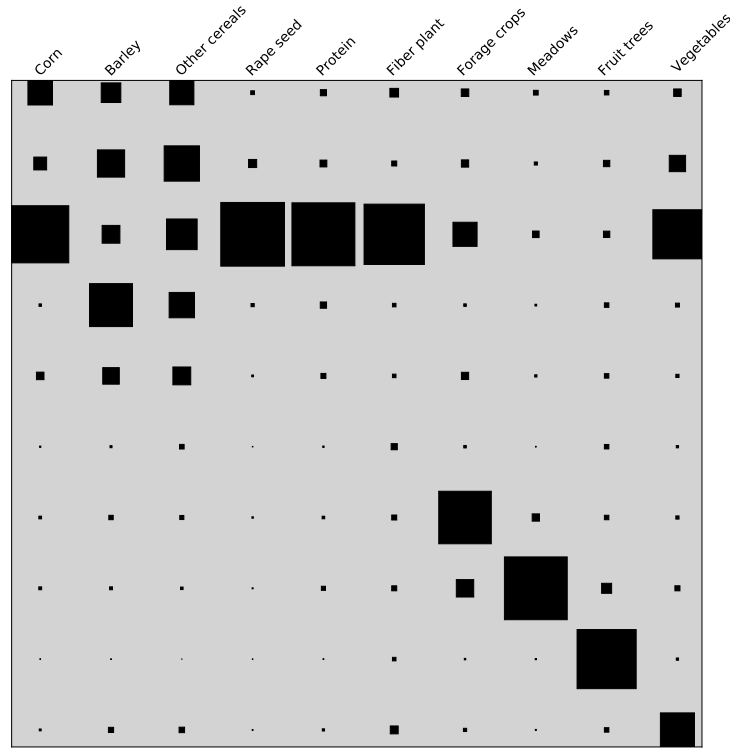


Figure 10: *Site 77* - Representation of the transition matrix with a Hinton diagram.

425 between one given year and the previous year. Figures 10 and 11 give the
 426 estimated transitions between crop classes as Hinton diagrams, for both sites.

427 On *Site04*, the most probable transitions are to and from permanent
 428 crops, such as *olive groves*, *vignards*, *orchards*, *estive landes*, *meadows* and
 429 *fruit trees* reaching 98.34%, 93.87%, 92.72%, 98.31%, 91.89% and 84.23%,
 430 respectively. From the transition matrix, we can observe that the standard
 431 rotation patterns of annual crops are generally not applied in this area. The
 432 *rape seed*, *proteins* and *sun flowers* have probabilities of 76.53%, 66.78% and
 433 64.25%, respectively to be transformed to *other cereals* the following year.

434 On *Site77*, the most probable transitions are conversely observed for the
 435 annual crops. Agronomical rules for annual crops rotation seems to be much
 436 more enforced in this area. The *rape seed* and *proteins* have probabilities
 437 of 97.09% and 94.85%, respectively to be transformed to *other cereals* the
 438 following year. The *rapeseed* \rightarrow *winter wheat* (in *other cereals*) \rightarrow *barley* is a

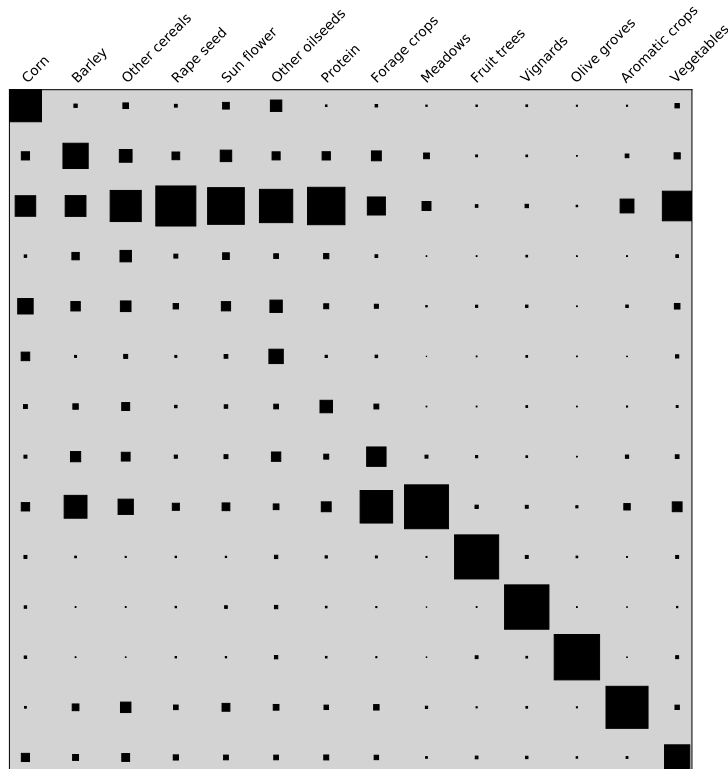


Figure 11: *Site 04* - Representation of the transition matrix with a Hinton diagram.

439 well-known 3-year rotation for farmers of this area. Permanent crops such as
 440 *meadows, orchards, fruit trees, vineyards* have a probability of being carried
 441 over the next year of 94.45%, 83.65%, 81.39% and 62.12%, respectively.

442 4.3. Quantitative and qualitative analysis

443 This section illustrates prediction accuracies using different feature combi-
 444 nations and both unstructured and structured approaches.

445 4.3.1. Quantitative evaluation on *Site04*

446 From the results displayed in Table 4, one can see that for parcel-based
 447 crop type prediction using image observations, optical data give better results
 448 than radar data (+9.1% for OA and +10.4% for weighted F-score). This can
 449 be explained by the finer resolution of optical imagery, as well as the small
 450 parcel size of *Site04* (*cf.* Section 4.3.2. Furthermore, *Site04* being situated

451 in sunny Southern France, it has generally little cloud cover, making optical
 452 data very available.

Table 4: Global prediction accuracies on *Site04*, using different feature and methodological configurations.

Unstructured			
Config	OA	F-score	Weighted F-score
Radar	0.639	0.587	0.610
Optical	0.730	0.669	0.714
Radar Optical	0.729	0.679	0.713
Structured			
Radar	0.757	0.592	0.698
Optical	0.776	0.627	0.725
Radar Optical	0.775	0.645	0.723

453 The results confirm that optical and radar combination leads to the best
 454 results in both unstructured and structured approaches. However, the global
 455 results remain low for this site, with F-scores varying between 0.58 and 0.64.
 456 This is due to the very small size of parcels and highly imbalanced classes.
 457 For example, parcels of permanent classes (*meadows*, *fruit trees*, *vignards*,
 458 *olive groves*) are overrepresented, as shown in Figure 4.

459 The confusion matrix for unstructured optical/radar configuration (Ta-
 460 ble 6) shows that most ambiguities occur on *meadows* classes, *other cereals* and
 461 *forage crops*. When integrating the temporal structure, the overall accuracy
 462 is improved by 4.6%. Moreover, while the OA using radar data is very low
 463 (63.9%), it is improved by the structured approach by 11.8%, confirming the
 464 impact of temporal structure even if the accuracy of the parcel-wise prediction
 465 is low.

466 In Table 5, we display the F-score, recall, and accuracy measures per class
 467 for both unstructured and structured approaches using radar and optical
 468 combination.

469 As for per-class accuracies, temporal structure highly improves the accu-
 470 racies of permanent crops (fruit trees +36%, vignards +29.7%, olive groves
 471 +25.6%, aromatic groves +19%) reaching F-scores higher than 92.9%. The
 472 F-score for *meadows* (permanent and temporary) is improved by 4.1%. These

Table 5: Effect of temporal structure on Classification metrics on *Site04*, using aggregated radar and optical attributes.

Class	Unstructured			Structured		
	F score	Recall	Precision	F score	Recall	Precision
Corn	0.888	0.953	0.832	0.780	0.836	0.732
Barley	0.393	0.848	0.256	0.185	0.673	0.107
Other cereals	0.846	0.830	0.862	0.783	0.730	0.845
Rape seed	0.923	1	0.857	0.712	1	0.554
Sun flower	0.789	0.785	0.793	0.713	0.749	0.681
Other oilseeds	0.570	0.745	0.463	0.408	1	0.258
Protein	0.484	1	0.321	0	0.0714	0
Forage crops	0.469	0.735	0.344	0.096	0.884	0.051
Meadows	0.759	0.675	0.867	0.800	0.674	0.983
Fruit trees	0.609	0.863	0.471	0.969	0.962	0.975
Vignards	0.690	0.740	0.646	0.987	0.996	0.979
Olive groves	0.737	0.819	0.670	0.993	0.997	0.989
Aromatic crops	0.739	0.646	0.864	0.929	0.938	0.921
Vegetables	0.611	0.725	0.529	0.674	0.891	0.542

473 results were expected since the permanent crops have the highest transition
474 probability as shown in Section 4.2.

475 However, F-scores of annual crops classes decrease when using temporal
476 structure; only slightly so for corn, other cereal, rape seed and sunflowers
477 but barley, other oilseeds, protein and forage crops are significantly more
478 misclassified (*cf.* table 6). This is due to the fact that the transitions of annual
479 crops are less stable and highly vary with regard to agricultural practices and
480 operators in this area.

481 4.3.2. Impact of parcel size on *Site04*

482 Figure 12 shows the impact of parcel size on parcel-wise global accuracies.
483 Since *Site04* is highly fragmented, when keeping only large parcels (area
484 >3 ha), the number of parcels is reduced by 77.5%. Overall accuracies are
485 highly improved by 15%, 5.9% and 8.7% for radar, optical and aggregated
486 optical/radar attributes, respectively). Indeed, due to the limited spatial
487 resolution of Sentinel-1 images, radar attributes are more sensitive to small

Table 6: Confusion matrices using aggregated optical and radar attributes on *Site04*.

	Corn	Barley	O. cereals	Rape Seed	Sun flower	O. oilseeds	Protein	Forage crops	Meadows	Fruit trees	Vignards	Olive groves	Arom crops	Vegetables
	Unstructured Optical radar													
Corn	31	-	-	-	1	2	-	-	-	-	1	-	-	3
Barley	-	47	9-	-	-	-	-	3	37	-	-	-	13	-
O. cereals	-	5	684	-	5	1	-	5	59	-	-	4	25	1
Rape seed	-	-	1	56	-	-	-	-	10	-	-	-	-	-
Sun flower	-	-	1	-	78	-	-	-	2	-	-	-	13	4
O. oilseeds	1	-	-	-	7	18	-	-	4	-	1	-	2	7
Protein	-	2	6	-	-	-	10	1	7	-	-	-	2	-
Forage crops	-	-	18	-	1	-	-	173	239	6	3	9	64	2
Meadows	-	3	16	-	3	1	-	47	1294	-	9	27	77	3
Fruit trees	1	-	1	-	-	-	-	-	52	56	1	9	5	-
Vignards	-	-	-	-	-	-	-	-	18	-	74	4	19	-
Olive groves	-	-	4	-	-	1	-	1	113	1	6	311	26	1
Arom crops	-	-	1	-	-	-	-	-	64	-	2	6	480	2
Vegetables	-	-	2	-	6	4	-	2	18	-	4	6	9	60
	Structured Optical radar													
Corn	28	-	7	-	1	-	-	-	1	-	-	-	1	-
Barley	-	20	123	-	-	-	-	-	47	-	-	-	-	-
O. cereals	1	1	676	-	2	-	-	-	1-2	-	-	-	6	1
Rape seed	-	5	21	35	-	-	-	-	6	-	-	-	-	-
Sun flower	-	-	6	-	67	-	-	1	13	-	-	-	8	3
O. oilseeds	4	-	4	-	7	10	-	-	14	-	-	-	-	1
Protein	-	2	21	-	-	-	-	-	5	-	-	-	-	-
Forage crops	1	-	15	-	3	-	-	25	461	-	-	-	9	1
Meadows	-	1	16	-	1	-	-	2	1456	-	-	1	3	-
Fruit trees	-	-	-	-	-	-	-	-	2	122	1	-	-	-
Vignards	-	-	-	-	-	-	-	-	3	-	112	-	-	-
Olive groves	-	-	1	-	-	-	-	-	3	2	-	458	-	-
Arom crops	-	1	17	-	-	-	-	-	26	-	-	-	511	-
Vegetables	-	-	20	-	10	-	-	-	16	3	-	-	4	58

488 parcel sizes. When considering parcels greater than 3 ha, radar OA reaches
 489 the optical OA at 79.3%.

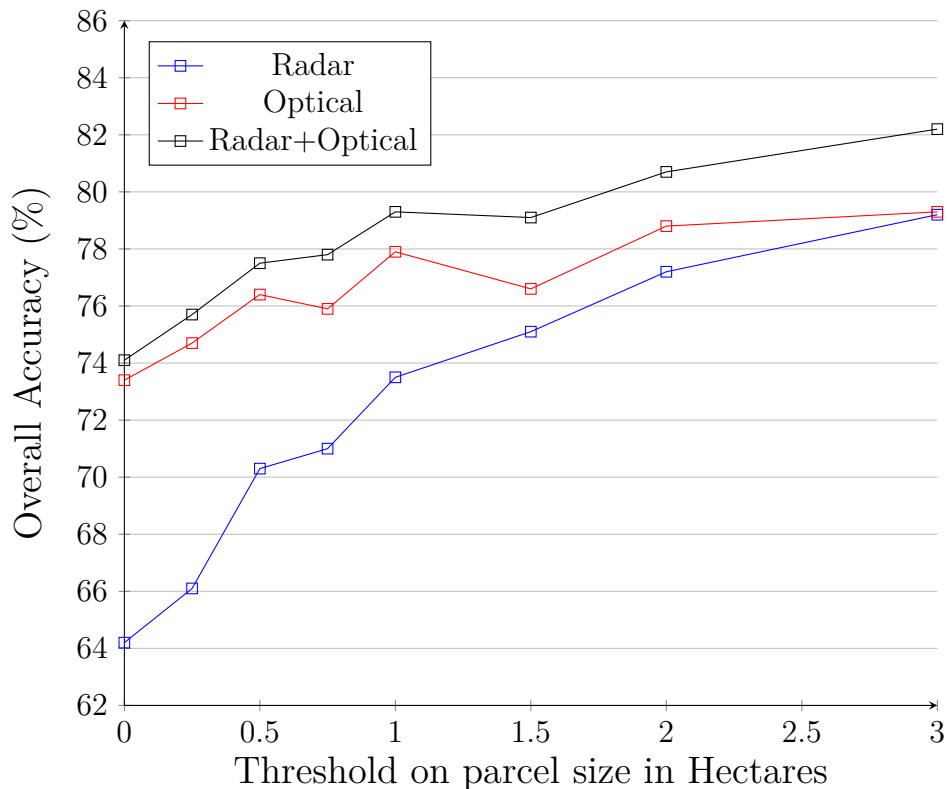


Figure 12: Impact of the parcel size on the global accuracy for parcel-wise classification on *Site04* in the year 2016. x-axis: only parcels whose surface area exceeds the threshold (in ha) are considered.

490 4.3.3. Quantitative evaluation on *Site77*

491 Overall accuracies and F-scores are displayed in Table 7. They are averaged
 492 over 10 runs of the random forest classifier. Contrarily to the previous site,
 493 on *Site77*, radar attributes give better results than optical attributes (OA =
 494 0.892 Vs. 0.824) for the unstructured approach. This is due to a combination
 495 of frequent acquisition problems and high cloud cover in 2016, leading to
 496 many missing optical Sentinel-2 data on this study area (cf. Figure 8). In
 497 addition, the parcels on *Site77* are larger and thus more compatible with
 498 radar Sentinel-1 image spatial resolution. However, aggregated optical and

499 radar attributes still give the best results for the unstructured approach.

Table 7: Global prediction accuracies on *Site77*, using different attribute and methodological configurations.

Unstructured			
Config	OA	F-score	Weighted F-score
Radar	0.892	0.734	0.878
Optical	0.824	0.624	0.809
Radar Optical	0.890	0.744	0.885
Structured			
Radar	0.919	0.776	0.911
Optical	0.870	0.675	0.853
Radar Optical	0.916	0.762	0.906

500 When looking at per-class accuracies in Table 8, one can see that unlike
 501 *Site04*, very good overall accuracies are obtained for annual crops (*Corn*
 502 (94.1%), *Barley* (89.8%), *Other cereals* (94.7%), *Rape seed* (95.9%), ...) with
 503 the exception of forage crops. Indeed this class is hard to classify using
 504 satellite imagery since it is an agronomic class, making it harder to identify
 505 using only spectral or radar scattering information even on temporal images.
 506 As with *Site04*, Table 8 shows that the *meadows* class is often confused with
 507 other classes, particularly *fruit trees* and other cereals. In this case, this is
 508 due to the combination of trees and bare soil found in *meadows*, which has a
 509 low volumetric radar response.

510 The structured approach improves overall accuracies by 2.7%, 4.6% and
 511 2.6% for radar, optical, and aggregated optical/radar attributes, respectively.
 512 The improvement of temporal structure is lower than for *Site04*, as the initial
 513 parcel-wise accuracies are already strong (OA>82%). However, one can
 514 observe that the structured approach leads to the best results with radar
 515 attributes only.

516 As for *Site04*, the best improvements occur on permanent crops such as
 517 meadows and fruit trees (cf. Table 9). Moreover, the temporal structure
 518 improves the prediction of some annual crops such as other cereals, Rape
 519 seeds and proteins since they have a high first order transition probability to
 520 other cereals.

Table 8: Effect of temporal structure on Classification metrics on *Site77*, using aggregated radar and optical attributes.

Class	Unstructured			Structured		
Class	F-score	Recall	Precision	F-score	Recall	Precision
Corn	0.941	0.929	0.953	0.878	0.831	0.935
Barley	0.898	0.937	0.862	0.816	0.785	0.849
Other cereals	0.947	0.956	0.9378	0.954	0.941	0.968
Rape seed	0.959	0.975	0.944	0.969	0.985	0.954
Protein	0.949	0.932	0.968	0.953	0.967	0.939
Fiber plants	0.974	1	0.950	0	0.1	0
Forage crops	0	0.1	0	0.705	0.778	0.648
Meadows	0.868	0.814	0.930	0.955	0.943	0.967
Fruit trees	0.010	0.090	0	0.940	1	0.892
Vegetables	0.895	0.914	0.877	0.451	0.970	0.297

521 4.3.4. Impact of parcel size on *Site77*

522 Figure 13 shows the impact of parcel size on the global accuracies of the
 523 parcel-wise prediction. Since *Site77* is less fragmented than *Site04*, keeping
 524 only large parcels (area > 3 ha), reduces the number of parcels by % 52,3%.

525 As with *Site04*, when considering larger parcels, the overall accuracy is
 526 greatly improved with radar attributes (by 7.3% reaching 97.1%), which
 527 confirms the high sensitivity of radar images to parcel size.

528 For optical attributes, the relation between parcel size and accuracy is
 529 less clear. This may be due to the data imbalance, with some classes that are
 530 more present in small parcels (0.5-1.5 ha) and which are well identified such
 531 as Rape seed or Protein. Thus, removing these small parcels may decrease
 532 the overall accuracy. The classes that are responsible for the higher OA
 533 observed between 0 and 0.75 ha are *Fiber plants* and *Meadows* where *meadows*
 534 parcels are much smaller than for other classes and that *fiber plants* parcels
 535 are homogeneous in terms of area (*cf.* Figure 5).

536 As for radar data sensitivity to limited parcel sizes, some improvements of
 537 our framework could be undertaken on radar pre-processing. Indeed, the GRD
 538 Sentinel-1 images were used as input images when each GRD radar pixel is
 539 already an average of 5 pixels of the SLC (Single Look Complex). Using SLC
 540 images directly would allow us to achieve greater spatial resolution. Then, a

Table 9: Confusion matrices using aggregated optical and radar attributes on *Site77*.

	Corn	Barley	Other cereals	Rape Seed	Fiber plants	Protein	Forage crops	Meadows	Fruit trees	Vegetables
Unstructured Optical radar										
Corn	119	-	-	-	-	-	-	6	-	-
Barley	1	48	2	-	1	-	-	3	-	-
Other cereals	-	2	309	-	-	-	-	19	-	1
Rape seed	-	-	-	38	-	-	-	3	-	-
Fiber plants	-	-	-	-	27	-	-	1	-	-
Protein	-	-	-	-	1	9	-	-	-	-
Forage crops	-	-	1	-	-	-	-	20	-	-
Meadows	10	1	9	1	-	-	-	276	-	1
Fruit trees	-	-	-	-	-	-	-	12	-	-
Vegetables	1	-	1	-	-	-	-	1	-	27
Structured Optical radar										
Corn	118	1	1	-	-	-	3	2	-	-
Barley	1	48	5	-	-	-	-	1	-	-
Other cereals	-	2	321	1	-	-	-	7	-	-
Rape seed	-	-	1	39	-	-	-	1	-	-
Fiber plants	-	-	1	-	27	-	-	-	-	-
Protein	1	8	-	-	1	-	-	-	-	-
Forage crops	-	1	2	-	-	-	13	5	-	-
Meadows	4	-	4	-	-	-	1	289	-	-
Fruit trees	-	-	-	-	-	-	-	-	12	-
Vegetables	19	-	2	-	-	-	-	-	-	9

541 simple speckle filter was used [30] on a restricted local neighborhood (5×5).
542 This is not a problem for large parcels as the radar scattering coefficients
543 are averaged afterwards at the agricultural parcel level. However, when
544 parcel surface areas approach the Sentinel-1 spatial resolution, this method
545 is no longer suitable. The robustness of adaptive radar speckle filtering to
546 small objects should be investigated [35]. Finally, using a very high spatial
547 resolution Digital Terrain Model instead of the SRTM could improve absolute

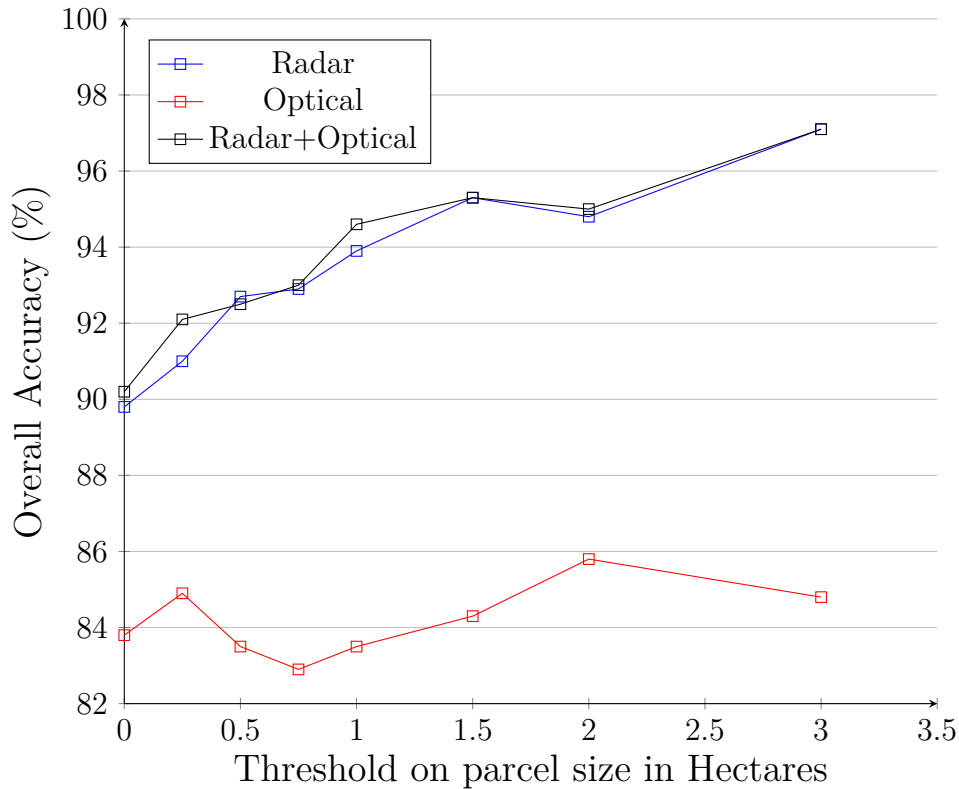


Figure 13: Unstructured parcel-based classification for year 2016, *Site77* - Impact of parcel size on accuracy; x-axis: only parcels whose surface area exceeds the threshold (in ha) are considered.

548 orthorectification accuracy of Sentinel-1 images and allows us to correct radar
 549 scattering coefficient from the effect of terrain slope (γ_0 calibration). As a
 550 result, the intra-class variability of signal could be reduced.

551 **5. Conclusion and perspectives**

552 This study demonstrated the efficiency of an automatic prediction of crop
 553 types using Sentinel 1 and 2 images and LPIS archives as a first step for an
 554 automatic filled pre-declaration intended for farmers.

555 From a thematic point of view, this paper demonstrates the efficiency
 556 of multi-temporal and multi-source Sentinel (optical and radar) images for
 557 crop type classification on two different sites. Very satisfactory discrimination
 558 results are obtained even with a large number of classes (>10). The remaining

559 limitations are essentially the parcel size with regard to the spatial resolution
560 of images and the complexity of the nomenclature. Results highlight the
561 high sensitivity of radar data to small parcel sizes, especially on *Site04*. This
562 issue can be reduced by a refining the preprocessing framework of radar data.
563 Moreover, the complexity of certain agronomic classes such as forage crops
564 should be discussed with agronomists in order to design a proper hierarchical
565 classification.

566 From a methodological point of view, we integrated the temporal structure
567 by automatically modeling the crop rotations using prevision editions of LPIS.
568 This model appears to be very efficient, improving the global classification
569 prediction of crop types. However, the impact of integrating temporal struc-
570 ture varies highly among classes. Although a positive impact is demonstrated
571 on permanent crops using first order crop transitions, this impact is fairly
572 limited or even detrimental for annual crops. Other transition orders should
573 be investigated to confirm the interest of temporal structure for annual crops.
574 Finally, thanks to the large volume of available LPIS data that can be used
575 as ground truth, and the free availability of numerous Sentinel images, deep
576 learning methods should be tested to learn parcels' embeddings.

577 Acknowledgments

578 The authors want to thank the ASP (French payment agency) and the
579 French agricultural ministry for the rich discussions and their guidance for
580 the nomenclature choice and crop rotation schemes.

581 References

- 582 [1] European Commission, Towards future Copernicus service components
583 in support to agriculture?, [https://ec.europa.eu/jrc/sites/jrcsh/
584 files/Copernicus_concept_note_agriculture.pdf](https://ec.europa.eu/jrc/sites/jrcsh/files/Copernicus_concept_note_agriculture.pdf), 2016.
- 585 [2] Y. Palchowdhuri, R. Valcarce-Diñeiro, P. King, M. Sanabria-Soto, Classi-
586 fication of multi-temporal spectral indices for crop type mapping: a case
587 study in coalville, uk, *The Journal of Agricultural Science* 156 (2018)
588 24–36.
- 589 [3] J. Inglada, M. Arias, B. Tardy, O. Hagolle, S. Valero, D. Morin, G. Dedieu,
590 G. Sepulcre, S. Bontemps, P. Defourny, et al., Assessment of an oper-
591 ational system for crop type map production using high temporal and

- 592 spatial resolution satellite optical imagery, *Remote Sensing* 7 (2015)
593 12356–12379.
- 594 [4] L. Breiman, Random forests, *Machine learning* 45 (2001) 5–32.
- 595 [5] M. Immitzer, F. Vuolo, C. Atzberger, First experience with Sentinel-2
596 data for crop and tree species classifications in central Europe, *Remote*
597 *Sensing* 8 (2016) 166.
- 598 [6] N. Kussul, G. Lemoine, F. J. Gallego, S. V. Skakun, M. Lavreniuk, A. Y.
599 Shelestov, Parcel-based crop classification in Ukraine using Landsat-8
600 data and Sentinel-1a data, *IEEE Journal of Selected Topics in Applied*
601 *Earth Observations and Remote Sensing* 9 (2016) 2500–2508.
- 602 [7] Sen2-Agri, Czech agriculture national demonstrator - final re-
603 port. [http://www.esa-sen2agri.org/wp-content/uploads/docs/
604 CzechAgri%20Final%20Report%201.2.pdf](http://www.esa-sen2agri.org/wp-content/uploads/docs/CzechAgri%20Final%20Report%201.2.pdf), 2018. Accessed on February
605 6, 2018.
- 606 [8] Z. Berzsenyi, B. Györfly, D. Lap, Effect of crop rotation and fertilisation
607 on maize and wheat yields and yield stability in a long-term experiment,
608 *European Journal of Agronomy* 13 (2000) 225–244.
- 609 [9] D. L. Karlen, E. G. Hurley, S. S. Andrews, C. A. Cambardella, D. W.
610 Meek, M. D. Duffy, A. P. Mallarino, Crop rotation effects on soil quality
611 at three northern corn/soybean belt locations, *Agronomy journal* 98
612 (2006) 484–495.
- 613 [10] D. Karlen, G. Varvel, D. G. Bullock, R. Cruse, Crop rotations for the
614 21st century, *Advances in agronomy* 53 (1994).
- 615 [11] S. Dogliotti, W. Rossing, M. Van Ittersum, ROTAT, a tool for system-
616 atically generating crop rotations, *European Journal of Agronomy* 19
617 (2003) 239–250.
- 618 [12] M. Castellazzi, G. Wood, P. J. Burgess, J. Morris, K. Conrad, J. Perry,
619 A systematic representation of crop rotations, *Agricultural Systems* 97
620 (2008) 26–33.
- 621 [13] J. Dury, N. Schaller, F. Garcia, A. Reynaud, J. E. Bergez, Models to
622 support cropping plan and crop rotation decisions. a review, *Agronomy*
623 *for sustainable development* 32 (2012) 567–580.

- 624 [14] J. Aurbacher, S. Dabbert, Generating crop sequences in land-use models
625 using maximum entropy and Markov chains, *Agricultural Systems* 104
626 (2011) 470–479.
- 627 [15] N. K. Detlefsen, A. L. Jensen, Modelling optimal crop sequences using
628 network flows, *Agricultural Systems* 94 (2007) 566–572.
- 629 [16] J. E. Olesen, M. Trnka, K. Kersebaum, A. Skjelvåg, B. Seguin,
630 P. Peltonen-Sainio, F. Rossi, J. Kozyra, F. Micale, Impacts and adapta-
631 tion of European crop production systems to climate change, *European*
632 *Journal of Agronomy* 34 (2011) 96–112.
- 633 [17] J. Aurbacher, P. S. Parker, G. A. C. Sánchez, J. Steinbach, E. Reinmuth,
634 J. Ingwersen, S. Dabbert, Influence of climate change on short term
635 management of field crops—a modelling approach, *Agricultural Systems*
636 119 (2013) 44–57.
- 637 [18] F. Le Ber, M. Benoît, C. Schott, J.-F. Mari, C. Mignolet, Studying
638 crop sequences with CarrotAge, a HMM-based data mining software,
639 *Ecological modelling* 191 (2006) 170–185.
- 640 [19] M. Schönhart, E. Schmid, U. A. Schneider, CropRota—a crop rotation
641 model to support integrated land use assessments, *European Journal of*
642 *Agronomy* 34 (2011) 263–277.
- 643 [20] J. Bachinger, P. Zander, ROTOR, a tool for generating and evaluat-
644 ing crop rotations for organic farming systems, *European Journal of*
645 *Agronomy* 26 (2007) 130–143.
- 646 [21] Y. Xiao, C. Mignolet, J.-F. Mari, M. Benoît, Modeling the spatial distri-
647 bution of crop sequences at a large regional scale using land-cover survey
648 data: A case from France, *Computers and Electronics in Agriculture*
649 102 (2014) 51–63.
- 650 [22] C. Boryan, Z. Yang, R. Mueller, M. Craig, Monitoring us agriculture:
651 the us department of agriculture, national agricultural statistics service,
652 cropland data layer program, *Geocarto International* 26 (2011) 341–358.
- 653 [23] B. Leteinturier, J. Herman, F. De Longueville, L. Quintin, R. Oger,
654 Adaptation of a crop sequence indicator based on a land parcel man-
655 agement system, *Agriculture, Ecosystems & Environment* 112 (2006)
656 324–334.

- 657 [24] J. Osman, J. Inglada, J.-F. Dejoux, Assessment of a Markov logic model
658 of crop rotations for early crop mapping, *Computers and Electronics in*
659 *Agriculture* 113 (2015) 234–243.
- 660 [25] L. Aurdal, R. B. Huseby, L. Eikvil, R. Solberg, D. Vikhamar, A. Solberg,
661 Use of hidden Markov models and phenology for multitemporal satellite
662 image classification: Applications to mountain vegetation classification,
663 in: *Proc. Int. Workshop Analysis Multi-Temporal Remote Sensing Images*,
664 pp. 16–18.
- 665 [26] P. B. C. Leite, R. Q. Feitosa, A. R. Formaggio, G. A. da Costa, O. Pedro,
666 K. Pakzad, I. D. Sanches, Hidden Markov Models for crop recognition in
667 remote sensing image sequences, *Pattern Recognition Letters* 32 (2011)
668 19–26.
- 669 [27] S. Siachalou, G. Mallinis, M. Tsakiri-Strati, A hidden Markov models
670 approach for crop classification: Linking crop phenology to time series of
671 multi-sensor remote sensing data, *Remote Sensing* 7 (2015) 3633–3650.
- 672 [28] C. Conrad, S. Dech, O. Dubovyk, S. Fritsch, D. Klein, F. Löw,
673 G. Schorcht, J. Zeidler, Derivation of temporal windows for accurate
674 crop discrimination in heterogeneous croplands of Uzbekistan using mul-
675 titemporal RapidEye images, *Computers and Electronics in Agriculture*
676 103 (2014) 63–74.
- 677 [29] B. Kenduiywoa, D. Bargiel, U. Soergel, Spatial-temporal Conditional
678 Random Fields crop classification from Terrasar-X images, *ISPRS Annals*
679 *of the Photogrammetry, Remote Sensing and Spatial Information Sciences*
680 2 (2015) 79.
- 681 [30] J.-S. Lee, Digital image enhancement and noise filtering by use of
682 local statistics, *IEEE Transactions on Pattern Analysis and Machine*
683 *Intelligence* (1980) 165–168.
- 684 [31] A. Veloso, S. Mermoz, A. Bouvet, T. Le Toan, M. Planells, J.-F. Dejoux,
685 E. Ceschia, Understanding the temporal behavior of crops using Sentinel-
686 1 and Sentinel-2-like data for agricultural applications, *Remote Sensing*
687 *of Environment* 199 (2017) 415–426.
- 688 [32] J. Inglada, OTB Gapfilling, a temporal gapfilling for image time series
689 library, Zenodo, 2016. [Http://doi.org/10.5281/zenodo.45572](http://doi.org/10.5281/zenodo.45572).

- 690 [33] D. Liu, K. Song, J. R. Townshend, P. Gong, Using local transition
691 probability models in Markov random fields for forest change detection,
692 Remote Sensing of Environment 112 (2008) 2222 – 2231.
- 693 [34] C. D. Manning, P. Raghavan, H. Schütze, et al., Introduction to in-
694 formation retrieval, volume 1, Cambridge university press Cambridge,
695 2008.
- 696 [35] C.-A. Deledalle, L. Denis, F. Tupin, A. Reigber, M. Jäger, NL-SAR:
697 A unified nonlocal framework for resolution-preserving (pol)(in) SAR
698 denoising, IEEE Transactions on Geoscience and Remote Sensing 53
699 (2015) 2021–2038.